

An infrared study of the double nucleus in NGC 3256

P. Lira,¹ G. Valentino,^{1,2} M. Ward,³ S. Hoyer,¹

¹ *Departamento de Astronomía, Universidad de Chile, Casilla 36-D, Santiago, Chile*

² *Department of Astronomy & Astrophysics, UC Santa Cruz, 201 Interdisciplinary Sciences Building, Santa Cruz, CA 95064, USA*

³ *Department of Physics, University of Durham, Science Laboratories, South Road, Durham DH1 3LE, UK*

14 December 2018

ABSTRACT

We present new resolved near and mid-IR imaging and N-band spectroscopy of the two nuclei in the merger system NGC 3256, the most IR luminous galaxy in the nearby universe. The results from the SED fit to the data are consistent with previous estimates of the amount of obscuration towards the nuclei and the nuclear star formation rates. However, we also find substantial differences in the infrared emission from the two nuclei which cannot be explained by obscuration alone. We conclude that the northern nucleus requires an additional component of warm dust in order to explain its properties. This suggests that local starforming conditions can vary significantly within the environment of a single system.

Key words: galaxies: general – galaxies: nuclei

1 INTRODUCTION

The dominance of obscured star formation in the early Universe makes the dusty nearby systems interesting laboratories in which to probe their physics and evolution. Because of their high level of obscuration, such studies are well suited to observations at near and mid-IR wavelengths. Our understanding of these sources has improved considerably since the IRAS era of the 1980's. This is partly due to the results from ISO in the 1990's and most recently from Spitzer. However, high spatial resolution is still not attainable from space facilities. This situation is, however, rapidly changing with the advent of new ground based instrumentation which is a valuable complement to the space missions.

Because of its closeness ($D \sim 39$ Mpc, for $H_0 = 70$ km s⁻¹ Mpc⁻¹) and luminosity ($L_{bol} \sim L_{IR} \sim 6 \times 10^{11} L_\odot$), NGC 3256 is one of the best studied Luminous Infrared Galaxies (LIRGs), note: it is almost a ULIRG! Its powerful infrared emission is the result of a merger of two massive galaxies, whose nuclei have a projected separation of only ~ 1 kpc, indicating an advanced stage of the collision.

NGC 3256 is also amongst the most X-ray luminous galaxies for which there is no clear evidence of the presence of a (luminous) active nucleus. In fact, the estimated luminosity of NGC 3256 ($L_x \sim 10^{42}$ ergs s⁻¹ in the 0.5–10 keV band - Lira et al., 2002; Moran, Lehnert & Helfand, 1999) is consistent with the maximum limit normally adopted to separate AGN from starburst galaxies found in deep X-ray surveys (see Alexander et al. 2005, and references therein.)

In this paper we present a study of the near and mid-IR

resolved emission from the two nuclei in the prototype LIRG NGC 3256. In section 2 we describe the high-spatial resolution, ground-based observations obtained in the N-band. In section 3 and 4 the details of our data analysis is presented. In Section 5 the SED of NGC 3256 is explored using our new N-band data, plus observations extracted from the literature and Spitzer and HST archival images. Finally, the discussion of our results is presented in Section 6.

2 OBSERVATIONS AND DATA REDUCTION

2.1 Imaging

The high-resolution N-band imaging of NGC 3256 was obtained with the Thermal Infrared MultiMode Instrument (TIMMI2) camera on the ESO 3.6m telescope at La Silla on the 24th of February 2001. A narrow N-band filter was used ($\lambda_c \sim 11.5\mu\text{m}$; $\Delta\lambda \sim 1.2\mu\text{m}$), and the image scale was 0.2'' per pixel. Standard chopping and nodding techniques were employed with perpendicular chop and nod throws of 15''. Despite the highly peaked light distribution centered on the nuclear region, it is expected that some galactic emission is also present $\sim 15''$ away from the nuclear sources. This might affect our ability to obtain an accurate sky subtraction, and is discussed further in Section 3.

The final image was constructed by shifting each individual frame onto a common reference position determined by using the centroid of the central source. The resulting exposure time was 1.16 ksecs. This image was flux calibrated using standard stars observed throughout the night. These

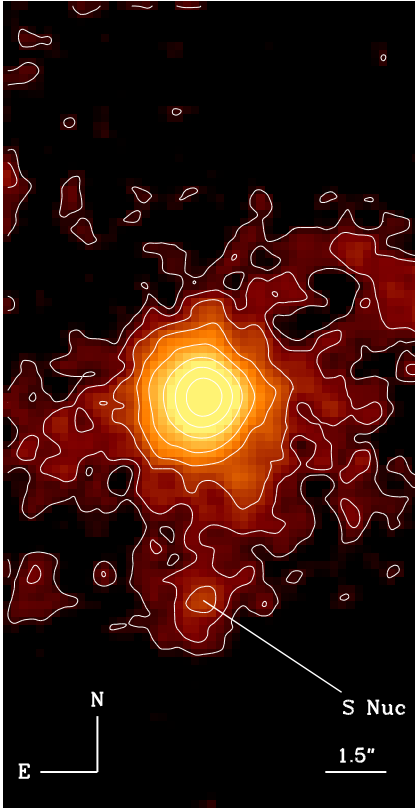


Figure 1. The high-resolution narrow N-band image ($\lambda_c \sim 11.5\mu\text{m}$) of the central region of NGC 3256 observed using TIMMI2. This image has been smoothed and displayed on a logarithmic scale. Clearly the emission is dominated by the northern nucleus, but the southern nucleus is also detected.

showed an RMS error of 8% in their fluxes. Inspection of the radial profile of the standard stars showed that the observations were diffraction-limited with a FWHM $\sim 0.8''$.

An uncalibrated, N-band $10.5\mu\text{m}$ image of NGC 3256 was published by Böker et al. (1997) as one of the first science images obtained with the MANIAC mid-IR camera. Siebenmorgen, Krügel & Spoon (2004) presented $8.6\mu\text{m}$ and $10.4\mu\text{m}$ imaging of this galaxy obtained with TIMMI2, but the detection of the southern nucleus is not discussed. Alonso-Herrero et al. (2006) have recently published a narrow-band, $8.7\mu\text{m}$ image of NGC 3256, and their measurements of the northern and southern nuclei will be used later in Section 5. We have also analysed archival Spitzer images of NGC 3256 (PI., Fazio). These observations were carried out with the IRAC camera in June 2004. The 'Post Basic Calibrated Data' were used to determine the photometry of the nuclei. Saturation affected the northern nucleus in the $8\mu\text{m}$ band images, and so these were not used. Finally, for the northern nucleus we also extracted the archival HST observations obtained using the WFPC2 camera with the F300W, F555W and F814W filters during June and Aug 2001 (PI's., Windhorst and van der Marel). We did not include the optical data published by Lípári et al. (2000)

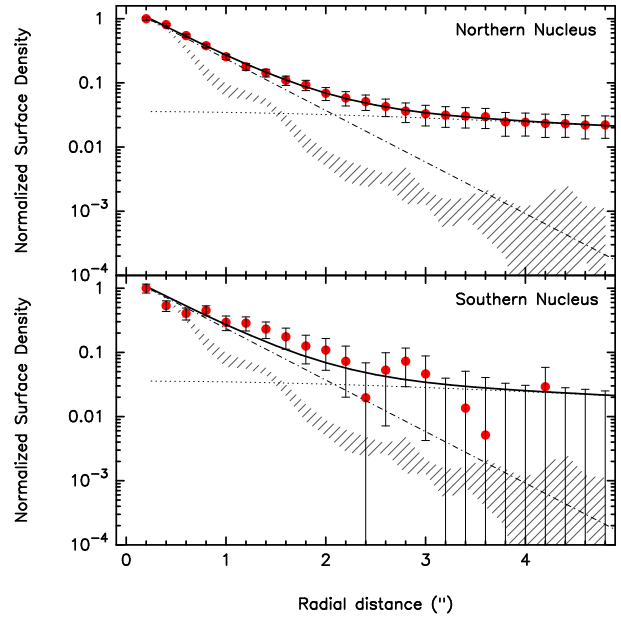


Figure 2. Normalized radial profiles of the two nuclei in NGC 3256. The profile of the southern nucleus was derived by using the lower half of the circular apertures centred on the nucleus, in order to avoid the strong contamination from the northern source. A 1σ interval in radial profiles of the standard stars observed during the same night are also included for comparison (hashed region). The extended profile of the northern nucleus was fitted using the sum of a lorentzian and exponential function (shown as a thin continuous line). The same fit is superimposed on the profile of the southern nucleus.

in our analysis because the used apertures and seeing conditions did not meet our requirements (see Section 5).

2.2 Spectroscopy

Long-slit N-band spectroscopy of NGC 3256 was obtained during the science verification phase of the TReCS camera on Gemini South on the 3rd of January 2004. The low resolution KBrC grating was used giving a spectral resolution $R \sim 100$ in the $8 - 12.5\mu\text{m}$ wavelength range. The slit width was $1.3''$ and was rotated to a nearly N-S position angle in order to cover both nuclei simultaneously. The chopping and nodding were performed in the direction perpendicular to the slit orientation, with a throw of $30''$. The total on-source integration time was 1.28 ksecs.

The images were reduced using the Gemini *midir* IRAF package, which derives background subtracted images from different chopping and nodding positions, then registers them and produces a final averaged image. Extraction of the spectra of both nuclei was performed using standard IRAF package routines. Due to the low S/N available for the southern nucleus, we used the trace function determined for the northern nucleus to extract this spectrum. Aperture photometry of the TIMMI2 image within a diameter of $1.3''$ has been used to determine a good absolute flux calibration for the spectra.

Spitzer-IRS observations of NGC 3256 have been published by Brandl et al. (2006) and are included in our analysis (Section 5). The observations were carried out on the 13th of May 2004 using the low-resolution module ($R \sim 65 - 130$).

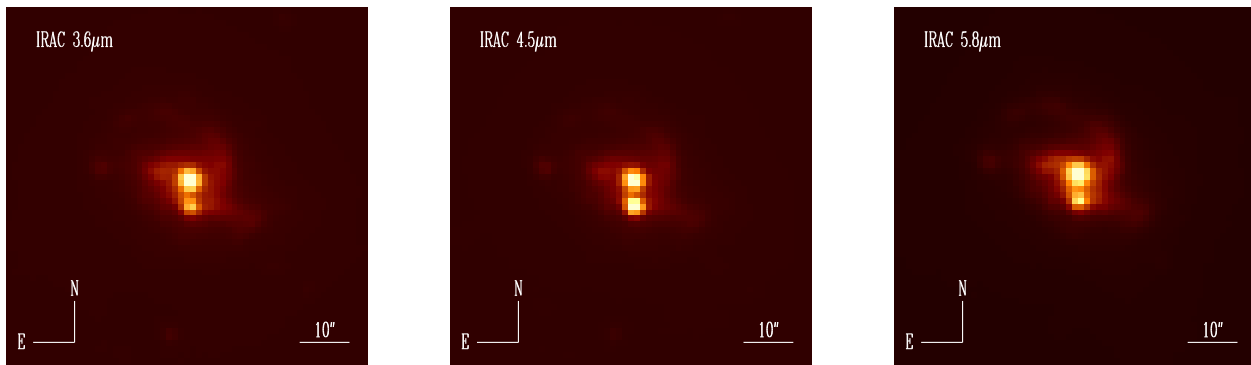


Figure 3. IRAC images of NGC 3256 in the 3.6, 4.5 and 5.8 μm bands.

The slit widths were $\sim 3.6''$ in the 5 – 15 μm range, and $\sim 10.5''$ for wavelengths greater than 15 μm , although the final flux calibration was obtained through the widest slit. Also, Martín-Hernández et al. (2006) have recently presented spatially resolved 7.5 – 13.9 μm spectroscopy of the double nuclei in NGC 3256 obtained with TIMMI2. Finally, Siebenmorgen, Krügel & Spoon (2004) presented TIMMI2 and ISO spectroscopy for this galaxy, but as was the case with their TIMMI2 imaging, there is no discussion of the possible detection of the southern nucleus.

3 IMAGE ANALYSIS

Figure 1 shows the TIMMI2 observations of the nuclear region in NGC 3256. The emission is clearly dominated by a central extended source, although other clumps of emission can be seen distributed around it. We identify the central source with the northern nucleus, while the much fainter source located $\sim 5''$ to the south, corresponds to the southern nucleus.

The radial profiles of both nuclei are shown in Figure 2. The northern nucleus is clearly extended when compared with a stellar PSF. A best fit to its profile was obtained by using a combination of an exponential and a lorentzian function. In order to reduce contamination from the northern nucleus in the photometry of the southern source, its profile was derived using photometry obtained from the lower-half of the circular apertures centred on this source. Despite the much lower signal-to-noise, it is clearly seen that the southern nucleus is also well resolved. Furthermore, the same fit that described the profile of the northern nucleus is also found to provide a good representation of the southern source. In fact the HST-NICMOS images show that the southern nucleus is the more extended of the two nuclei at near-IR wavelengths (Lira et al., 2002).

Photometry calculated within an aperture of $3''$ diameter centred on the northern and southern nuclei, gives fluxes of ~ 0.8 and ~ 0.1 Jy, respectively (see Table 1). Despite our efforts to reduce the contamination from the northern nucleus in the southern aperture, we must consider the flux from the southern nucleus to be uncertain. The total emission within an aperture of $9.5''$ in diameter centred on the

northern peak corresponds to 1.8 Jy. However, since the background subtraction of the image was obtained using a chopping throw of only $15''$, it is important to quantify the possibility of sky oversubtraction which could affect these measurements.

The total emission measured from the TIMMI2 image can be compared with the IRAS 12 μm ($\Delta\lambda = 8.5 - 15 \mu\text{m}$) photometry obtained by Sanders et al. (1995). For an IRAS beam of $0.77'$ in diameter they measured a marginally resolved source with a total flux of 3.6 Jy, which corresponds to a corrected flux of ~ 5 Jy in the 10.9 – 12.1 μm TIMMI2 band, if the northern nucleus best-fit model presented in Section 5 is adopted, and this model is representative of the emission from the whole region. Hence, the IRAS observations provide an estimate of the size of the total emitting region, which is comparable to the IRAS beam.

If we assume that the differences between the IRAS and the TIMMI2 fluxes are due to emission evenly distributed within an annular region of inner and outer diameters $9.5''$ and $0.77'$, respectively, then the corresponding surface brightness would be ~ 2 mJy/arcsec². This would correspond to corrections of $\sim 2\%$, $\sim 15\%$, and $\sim 10\%$ respectively to the fluxes for the total, northern and southern regions presented in Table 1 (see 3 last entries). However, it is quite possible that the emission from outside the TIMMI2 image does not follow a completely even distribution, but instead has a steep profile. To test this scenario we extrapolated the fitted profile shown in Figure 2 out to the region used for the sky subtraction ($\sim 15''$ away). The estimated value is only ~ 0.3 mJy/arcsec². Again, this result suggests that our measurements do not suffer from a severe background oversubtraction. Integrating the fit to the profile of the northern nucleus out to a diameter of $0.77'$ underestimates the observed IRAS flux by $\sim 60\%$, suggesting that the larger scale surface brightness (i.e., that lying outside the TIMMI2 image) is actually closer to the flat distribution that we proposed earlier.

Figure 3 presents the IRAC images in the 3.6, 4.5 and 5.8 μm bands. The spatial resolution of IRAC (FWHM $\sim 1.5''$) clearly separates the two nuclei. It can be seen that in the 4.5 μm band image the two nuclei have a very similar peak brightness, while the northern nucleus is more prominent at 3.6 and 5.8 μm .

Table 1. Aperture photometry of the two nuclei in NGC 3256. Errors correspond to 2% for the WFPC2, 15% for the IRAC, and 8% for the TIMMI2 measurements. Kotilainen et al. (1996) report errors of 5% for JHK' and 10% for the L'-band photometry, respectively. See text for details of the used apertures.

Wave.	Ap. (")	North (mJy)	South (mJy)	Source/Reference
2924 Å	3.0	0.45 ± 0.01	–	WFPC2 F300W - this work
5252 Å	3.0	2.79 ± 0.06	–	WFPC2 F555W - this work
8269 Å	3.0	7.02 ± 0.14	–	WFPC2 F814W - this work
1.25 μm	3.0	21.6 ± 1.1	4.7 ± 0.2	Kotilainen et al. (1996)
1.65 μm	3.0	33.2 ± 1.7	9.0 ± 0.4	Kotilainen et al. (1996)
2.10 μm	3.0	33.7 ± 1.7	10.5 ± 0.5	Kotilainen et al. (1996)
3.6 μm	3.6	33.5 ± 5.0	16.8 ± 2.5	IRAC band-1 - this work
3.75 μm	3.0	32.3 ± 3.2	24.8 ± 2.5	Kotilainen et al. (1996)
4.5 μm	3.6	30.0 ± 4.5	26.0 ± 3.9	IRAC band-2 - this work
5.8 μm	4.0	128 ± 19	71 ± 11	IRAC band-3 - this work
8.74 μm	1.4*	230 ± 11	40 ± 3	Alonso-Herrero et al. (2006)
11.5 μm	1.3†	350 ± 28	26 ± 2	TIMMI2 - this work
11.5 μm	3.0	810 ± 65	86 ± 7	TIMMI2 - this work
11.5 μm	9.5	1800 ± 144	–	TIMMI2 - this work

* A factor 1.4 is required to correct these fluxes to a $\sim 3.0''$ aperture.

† Used to derive the absolute calibration for the TReCS spectroscopy (see Fig. 4).

Ptak et al. (2006) and Taylor-Mager et al. (2007) have recently presented the archival WFPC2 data used in this work to obtain the optical photometry for the northern nucleus. Also, a spectacular WFPC2 colour image of NGC 3256 can be found in Zepf et al. (1999).

The TIMMI2, IRAC and WFPC2 photometry is given in Table 1. The IRAC photometry was obtained in apertures that roughly correspond to the same spatial region as measured in the $3.0''$ TIMMI2 aperture photometry. This was achieved by deconvolving the TIMMI2 image of the northern nucleus (using a standard star observation) and then convolving it with the characteristic FWHM for each IRAC band. Finally, an aperture size was defined so that the same fractional flux as that measured from the TIMMI2 image would be obtained. We assumed that the same IRAC apertures apply for the photometry of the southern nucleus. Given the small FWHM of the WFPC2 camera ($\sim 0.15''$) a $3.0''$ aperture was directly applied to obtain the optical photometry for the northern nucleus.

4 SPECTRAL ANALYSIS

The N-band spectra of the northern and southern nuclei in NGC 3256 are shown in Figure 4. Both spectra are flanked by the rising PAH features at $7.7 \mu\text{m}$ and the narrow [NeII] $\lambda 12.8 \mu\text{m}$ emission line which is blended with the $12.7 \mu\text{m}$ PAH feature. Unfortunately the [NeII] $\lambda 12.8 \mu\text{m}$ line is not completely covered in the spectral range of our data but it can be clearly seen in the data of Martín-Hernández et al. (2006).

The nuclear region of NGC 3256 was observed with the Spitzer IRS spectrograph. As can be seen in Figure 4, the IRS spectrum is a very good match to the TReCS observations of the northern nucleus, which clearly dominates the emission in the mid-IR (see Figure 1). Since the flux calibration of the IRS spectrum was obtained from a much larger aperture ($10.5''$), a scaling factor of 0.18 had to be applied to these data. This is also similar to the ratio between the

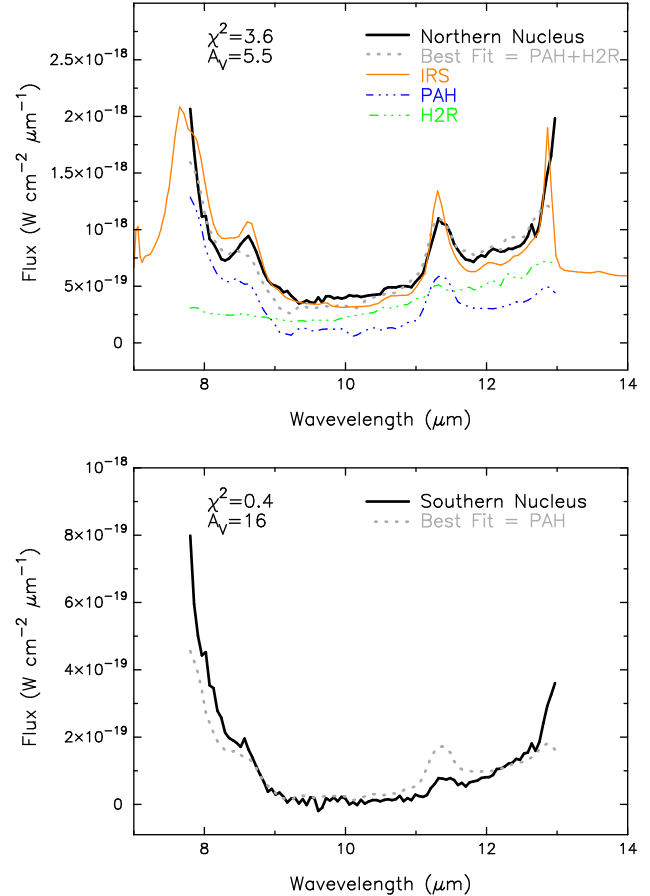


Figure 4. N-band spectra of the nuclei in NGC 3256. Absolute flux calibration was obtained using N-band photometry measured in $1.3''$ diameter apertures (see Table 1). The Spitzer IRS spectrum obtained by Brandl et al. (2006) is overplotted on the TReCS observations for the northern nucleus, after applying a scaling factor of 0.18.

Table 2. Results from the spectral fitting. The percentage contributions of each component to the integrated 8-12.5 μm flux are presented.

Nucleus	χ^2	Fixed A_V	PAH	HIIR	AGN
North	3.6	5.5	$\sim 55\%$	$\sim 45\%$	0%
South	0.4	16.0	100%	0%	0%

1.3'' and 9.5'' fluxes measured in the apertures applied to the TIMMI2 images, and presented in Table 1.

Following the model proposed by other authors (e.g., Laurent et al., 2000; Sturm et al., 2000), we assume a simple description of the N-band emission, and fitted the spectra of both nuclei as a combination of several components:

$$F_\lambda = \{C_1 F_\lambda^{HIIR} + C_2 F_\lambda^{PAH} + C_3 F_\lambda^{AGN}\} \times 10^{-A_\lambda/2.5}$$

where F^{HIIR} and F^{PAH} are empirical templates of an HII region and a PAH-dominated PDR region (Peeters, Spoon & Tielens, 2004). The F^{AGN} term is a template of a type 2 AGN, i.e., it corresponds to the reprocessed emission from the dusty torus without the directly visible contribution from an active nucleus. These templates were taken from Sturm et al. (2000) and Le Floc'h et al. (2001). A_λ is the assumed extinction curve. We have used the mid-IR extinction curves published by Draine (2003). C_1 , C_2 , and C_3 are free parameters which are determined by using χ^2 minimization and the σ spectrum, which is dominated by background emission.

Since the spectral range of our data is too narrow to allow us to determine the strength of the continuum, the PAH features and the extinction (which includes the silicate absorption at $\sim 9.8\mu\text{m}$), we have instead assumed a fixed value for the normalization of the extinction curve, (A_V). Since our spectra were obtained using a $\sim 1''$ slit, we have adopted $A_V = 5.5$ for the northern nucleus and $A_V = 16$ for the southern nucleus, as was determined from the 0.3'' resolution NICMOS images (Lira et al., 2002). These values are rather uncertain, since they were determined by assuming an intrinsic $H - K$ color for the starburst region. The same method gives $A_V = 2.5$ and $A_V = 5.3$ magnitudes for the northern and southern nuclei respectively, when the colours are measured from a 3'' aperture, while the use of a correlation between the radio 6 cm and [FeII] fluxes implies $A_V = 7.8$ and $A_V = 10.7$ for the northern and southern nuclei respectively (Kotilainen et al., 1996).

The outcome from the spectral fitting is summarized in Table 2. A clear result is that the northern nucleus shows a strong continuum contribution, while the southern nucleus is dominated by PAH emission, without the need for a significant continuum component. We have explored adopting lower values of A_V when fitting the spectrum of the southern source. In particular, in Section 5 we derive an extinction of $A_V = 10$ for this nucleus. However, these changes have very little impact on the best fit results.

Our fit suggests that the continuum of the northern nucleus has a stellar origin (F^{HIIR}), although if only an AGN continuum is allowed for the fit, then the result is also acceptable ($\chi^2 \lesssim 4$). However, the presence of an AGN in NGC 3256 is not supported by the very considerable body of observational evidence which indicates that an active nu-

Table 3. Flux and EW for the 11.3 μm PAH emission band.

Instrument	Slit (")	Flux ($\times 10^{-20}$ W/cm 2)	EW (μm)	Ref.
Northern nucleus				
TIMMI2	1.2	25	—	1
TReCS	1.3	17	0.3	2
TIMMI2	3.0	30	0.4	3
IRS	10.5	85	0.5	4
IRS	10.5	120	0.4	2
ISO	24.0	107	1.0	3
Southern nucleus				
TIMMI2	1.2	5	—	1
TReCS	1.3	2	0.7	2

Refs: 1 - Martín-Hernández et al., 2006; 2 - this work;
3 - Siebenmorgen et al., 2004; 4 - Brandl et al., 2006.

cleus is not present in this galaxy, or at least if it exists at all it is not the main component responsible for the powerful IR and X-ray emission (Doyon et al., 1994; Kotilainen et al., 1996; Moorwood & Oliva 1994; Norris & Forbes, 1995; Rigopoulou et al., 2000; L  pari et al., 2000; Lira et al., 2002; Verma et al., 2003).

We have also measured the flux and equivalent width of the 11.3 μm PAH feature clearly seen in both our spectra. Since it is not possible to easily unblend this emission from the neighbouring 12.7 μm PAH band and strong [NeII] λ 12.8 μm line, we have derived these measurements by simply assuming the continuum level to be a straight line from 10.9 μm to 11.7 μm . We compare our measurements with those from the literature in Table 3. In general there is good agreement between values obtained through similar slit widths, given the uncertainties in the absolute flux calibrations for spectroscopy and the different adopted continuum levels. In particular, we have re-analysed the IRS data using the continuum fit as defined above.

5 MODELLING THE SPECTRAL ENERGY DISTRIBUTION (SED)

In Figure 5 we show the SEDs for the nuclei in NGC 3256. Optical WFPC2 photometry is presented for the northern nucleus only. For both nuclei we have included near-IR fluxes from Kotilainen et al. (1996), the IRAC photometry, narrow-band Gemini-TReCS observations at 8.74 μm from Alonso-Herrero et al. (2006), and our new TIMMI2 observations.

For construction of the SEDs we aimed to use fluxes obtained from a spatial region closely corresponding to the 3'' diameter apertures used for our TIMMI2 imaging, which is characterised by a diffraction limited FWHM $\sim 0.8''$. This is already the case for the NIR data taken from Kotilainen et al. (FWHM $\sim 0.8 - 1''$). The WFPC2 and IRAC photometry presented in Section 3 also correspond to effective 3'' diameter apertures. Similar to the analysis performed to determine the IRAC photometry, we estimate that a factor 1.4 is necessary to correct the photometry presented in Alonso-Herrero et al. using a 1.4'' diameter aperture (with a resolution of $\sim 0.3''$) to 3''. All results from the aperture photometry are presented in Table 1.

The TReCS spectra are overplotted on the SEDs in Fig-

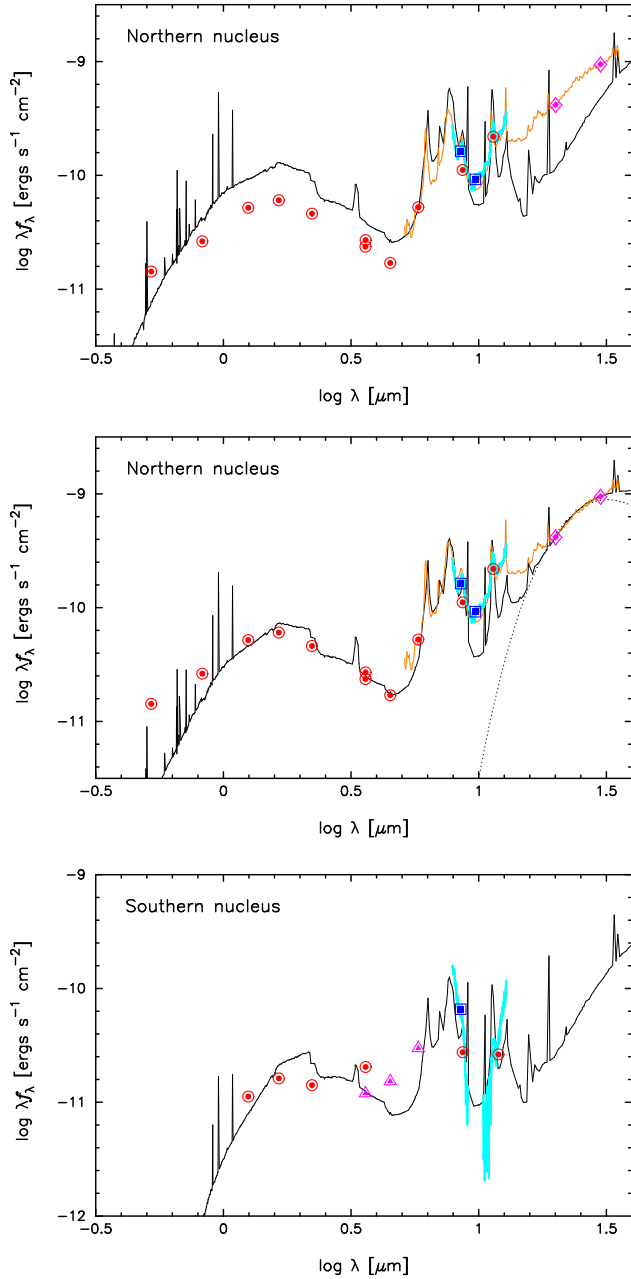


Figure 5. SED for the nuclei in NGC 3256. The top and middle panels show a fit to the northern nucleus (including a Gray Body component in the middle panel – dotted line), while the lower panel shows a fit to the southern nucleus. Optical, NIR and MIR aperture photometry is shown by circles (see Table 1). The mid-IR TReCS (and for the northern nucleus, IRS) spectra, scaled to the observed $3''$ diameter aperture TIMMI2 fluxes, are also shown with a thick and thin line, respectively. The spectra were binned to add further points to the SEDs (squares for TReCS data; diamonds for IRS data). Starburst models were taken from the work of Dopita et al. (2005).

Figure 5 after scaling them to the TIMMI2 flux observed in a $3''$ aperture (see Table 1). The IRS spectrum was included only for the northern nucleus after applying a scaling factor of 0.44. Given the good match between the TReCS and IRS spectra in the $8 - 12.5\mu\text{m}$ wavelength range (see Figure 4), we have assumed that the northern nucleus is also respon-

sible for most of the IRS flux at wavelengths longer than $13\mu\text{m}$. As discussed before, all photometric measurements were corrected to correspond to fluxes predicted within a $\sim 3''$ aperture.

Kotilainen et al. (1996) showed that the southern nucleus becomes relatively more prominent at longer wavelengths, and is comparable to the northern nucleus in the L-band. They interpreted this difference as being due to different amounts of dust obscuration towards the two nuclei. However our N-band data show a very weak southern nucleus when compared with the northern source, which is not consistent with such an explanation. In addition the IRAC observations presented in Figure 3 confirm this trend. The measured fluxes clearly show that their emission is very nearly the same at $\sim 4.5\mu\text{m}$, but diverge longwards and shortwards of this wavelength (see Table 1).

We performed an unweighted fit to the SEDs using the models presented by Dopita et al. (2005), which include a self-consistent treatment of dust re-emission from a starburst region. We also added extinction from a foreground screen of dust which was parameterised using the Calzetti et al. (2000) extinction law, ranging from the optical to $2.2\mu\text{m}$, and the Draine et al (2003) extinction curves from $2.2\mu\text{m}$ longwards. The best fit models imply visual band extinctions of ≈ 5 and ≈ 10 mags for the northern and southern nuclei, respectively. This is in good agreement with the previous determinations discussed in Section 4 within the uncertainties. These are mainly due to the assumption that a screen of foreground dust can account for the extinction towards the nuclei all the way from the optical to the mid-IR, since the geometry of these regions is probably more complex. Also, the adoption of a particular extinction curve would have some impact on the final determined extinction, while the templates used in our description of the spectra might not properly describe the intrinsic emission.

The starburst models have two free parameters, the ISM pressure (with $P/k = 10^4, 10^6$ and $10^7 \text{ cm}^{-3} \text{ K}$) and the characteristic time scale for the ‘clearing’ of the starforming regions (i.e., the time required for the covering factor of the star-forming clouds to decrease from 0.9 to 0.1). Changes in the pressure affect the model SEDs for fluxes above $\sim 15\mu\text{m}$ and therefore are not well constrained by our SED data. However, Rigopoulou et al. (1996) have determined an electron density $\sim 300 - 400 \text{ cm}^{-3}$ for the central region in NGC 3256, and therefore we considered those SED models corresponding to $P/k = 10^{6-7} \text{ cm}^{-3} \text{ K}$. The best fit models imply clearing times between 16 – 32 Myr for both nuclei.

Generally the starburst models provide a good match to the SEDs. The northern nucleus, however, clearly requires an extra component in its continuum at $\gtrsim 10\mu\text{m}$, as can be seen by comparing the top and middle panels in Figure 5. This is in agreement with our findings from the spectral analysis. The reprocessing of emission absorbed by foreground dust is not expected to contribute significantly at these wavelengths as the characteristic temperature of this emission would be lower than 50 K. Instead we have modelled the excess flux as a Gray body assuming an emissivity with index $\beta = -1.5$. The best fit temperature for this component is $\sim 80 \text{ K}$. The origin of this emission could be explained if the actual distribution of dust grain sizes is different to the one used in Dopita’s models. If this interpretation is correct then the excess emission is due to a com-

paratively larger contribution from very small dust grains, which dominate the dust re-emission in the mid-IR (Désert, Boulanger & Puget, 1990).

6 DISCUSSION

The normalization of the starburst SED models allow us to infer a star formation rate (SFR) of ~ 15 and $\sim 6M_{\odot}/\text{yr}$ for the northern and southern nuclei, respectively. This estimation does not take into account the Gray-body component added to the fit of the northern nucleus since its integrated luminosity corresponds to $\lesssim 25\%$ of the total emission. These SFRs are in good agreement with the values obtained using the supernova rate of 0.3 yr^{-1} per nucleus derived from radio observations (Norris & Forbes 1995) by assuming a conversion $\text{SNR} = 0.02 \times \text{SFR}$ as inferred from the Starburst 99 models using a constant star formation episode (Leitherer et al., 1999).

One of the interesting results obtained from our new N-band data is establishing the photometric and spectroscopic differences between the northern and southern nuclei, which cannot be explained simply by differences in dust obscuration. Since the starburst activity in these nuclei must have been triggered by the merger of two progenitors, the age of the starbursts is likely to be comparable, but other physical parameters could be different in the two separate merging parent galaxies.

X-ray, optical and near-IR observations are indicative of a highly obscured southern nucleus which is completely hidden at visible wavelengths but which becomes increasingly prominent in the near-IR. The brightness of the two peaks are comparable at $\sim 4\mu\text{m}$ and at radio wavelengths. Hence, it might be anticipated that in the mid-IR, where extinction becomes negligible, the two nuclei would also have similar flux levels. But this is not observed. Instead, we find that the northern nucleus exhibits excess continuum emission at wavelengths $\gtrsim 10\mu\text{m}$ when compared with the southern nucleus and with our model SEDs.

Interestingly a similar behaviour was found by Alonso-Herrero et al. (2006) when comparing the $8\mu\text{m}$ and $\text{Pa}\alpha$ emission from a sample of LIRG nuclei, including NGC 3256. While the northern nucleus shows a high $8\mu\text{m}/\text{Pa}\alpha$ ratio, as was also seen in other LIRGs, the lower $8\mu\text{m}/\text{Pa}\alpha$ value of the southern nucleus is consistent with the ratios observed in HII regions. Alonso-Herrero et al. (2006) explain this difference by the presence of large scale diffuse emission, which is characterised by strong PAH features in the mid-IR. As can be seen in Table 3, for NGC 3256 the EW of the $11.3\mu\text{m}$ PAH feature changes at most by a factor 3 between small ($11.2\text{--}1.3''$) and large ($10.5\text{--}24''$) apertures, while the line fluxes are greater by a factor ~ 6 . This suggests that the fractional increase in the continuum flux is also substantial (factor $\gtrsim 2$). In addition, the data presented in Figures 4 and 5 suggest that a significant fraction of the excess mid-IR flux is due to continuum emission produced by warm dust, heated in-situ by the starburst itself.

Using Spitzer IRS observations, Brandl et al. (2006) has quantified the continuum fluxes at 6, 15 and $30\mu\text{m}$ for a sample of starburst galaxies, including NGC 3256. Brandl's observations show that the flux ratio $F_{6\mu\text{m}}/F_{15\mu\text{m}} = 0.14$ determined for NGC 3256 is significantly lower than the av-

erage $\langle F_{6\mu\text{m}}/F_{15\mu\text{m}} \rangle = 0.26$ found for their starburst sample. As we have shown, the northern nucleus is more luminous than the southern nucleus by a factor of ~ 2 at $5.8\mu\text{m}$, while at $15\mu\text{m}$ the flux should be dominated by the northern nucleus. Indeed, using the best fit SEDs we find $F_{6\mu\text{m}}/F_{15\mu\text{m}} = 1.2$ for the southern nucleus, while for the northern nucleus we adopt the value tabulated from the IRS spectrum. The full range of observed flux ratios in Brandl's sample is $\sim 0.1 - 0.6$, which probably reflects the range in starburst conditions, such as age and dust properties. We find that the nuclei in NGC 3256 are representative of the two extremes of this distribution, but are found in the same central region of a single galaxy.

Finally we compare the $10.5\mu\text{m}$ and (unabsorbed, 2-10 keV) X-ray fluxes for both nuclei with the correlation derived by Krabbe, Böker & Maiolino (2001) using N-band MANIAC observations. The X-ray fluxes correspond to 9×10^{-17} and $4 \times 10^{-17} \text{ W m}^{-2}$ (Lira et al., 2002), while the $10.5\mu\text{m}$ fluxes ($\Delta\lambda = 5\mu\text{m}$, assuming the best fit SEDs) are ~ 400 and $\sim 40 \text{ mJy}$, respectively. It is found that both nuclei are X-ray deficient given their N-band photometry. In particular, because of its high mid-IR flux, the northern nucleus becomes a clear outlier in this correlation. But as shown by Krabbe's work, this is not the case for NGC 3256 when the fluxes are integrated over a large region, implying that the correlation holds for global starburst properties, but individual regions can show a much wider range of properties. In particular, our work shows that in-situ dust heating in LIRGs, whose emission can dominate the mid-IR emission, can be confined to very compact (few hundred-pc scale) regions.

ACKNOWLEDGEMENTS

P.L. and V.G. are grateful of support by the Fondecyt project No 1040719. We would like to thank Dr. B. Brandl for kindly supplying the IRS observations. We also wish to thank an anonymous referee for useful comments.

REFERENCES

- Alexander, D. M., Bauer, F., Chapman, S., Smail, I., Blain, A., Brandt, W. & Ivison, R. J., 2005, *ApJ*, 632, 736
- Alonso-Herrero, A., Colina, L., Packham, C., Diaz-Santos, T., Rieke, G., Radomski, J. & Telesco, C. M., 2006 *ApJL*, 652, L83
- Böker, T., Storey, J. W. V., Krabbe, A. & Lehmann, T, 1997, *PASP*, 109, 827
- Brandl B. R. et al., 2006, *ApJ* 653, 1129
- Calzetti, D., Armus, L., Bohlin, R. C., Kinney, A. L., Koornneef, J., Storchi-Bergmann, T., 2000, *ApJ*, 533, 682
- Désert, F.-X., Boulanger, F. & Puget, J. L., 1990, *A&A*, 237, 215
- Dopita, M. A., Groves, B. A., Fischera, J., Sutherland, R. S., Tuffs, R. J., Popescu, C. C., Kewley, L. J., Reuland, M., Leitherer, C., 2005, *ApJ*, 619, 755
- Doyon R., Joseph R. D. & Wright G. S., 1994, *ApJ*, 421, 101
- Draine, B. T., 2003, *ARA&A*, 41, 241
- Galliano, E., Alloin, D., Pantin, E., Lagage, P. O. & Marco, O., 2005, *A&A*, 438, 803
- Kotilainen J.K., Moorwood A.F.M., Ward M.J. & Forber D.A., 1996, *A&A*, 305, 107
- Krabbe, A., Böker, T. & Maiolino, R., 2001, *ApJ*, 557, 626

- Laurent, O., Mirabel, I. F., Charmandaris, V., Gallais, P., Madden, S. C., Sauvage, M., Vigroux, L. & Cesarsky, C., 2000, *A&A*, 359, 887
- Le Floc'h, E., Mirabel, I. F., Laurent, O., Charmandaris, V., Gallais, P., Sauvage, M., Vigroux, L. & Cesarsky, C., *A&A*, 2001, 367, 487
- Leitherer C. et al., 1999, *ApJS*, 123, 3
- Lípari S., Díaz R., Taniguchi Y., Terlevich R., Dottori H. & Carranza G., 2000, *AJ*, 120, 645
- Lira, P., Ward, M., Zezas, A., Alonso-Herrero, A. & Ueno, S., *MNRAS*, 2002, 330, 259
- Moran E.C., Lehnert M.D. & Helfand D.J., 1999, *ApJ*, 526, 649
- Martín-Hernández, N. L., Schaerer, D., Peeters, E., Tielens, A. G. G. M. & Sauvage, M., 2006, *A&A*, 455, 853
- Moorwood A. F. M. & Oliva E., 1994, *ApJ*, 429, 602
- Neff, S. G., Ulvestad, J. S. & Campion, S. D., 2003, *ApJ*, 599, 1043
- Norris R.P. & Forbes D.A., 1995, *ApJ*, 446, 594
- Peeters, E., Spoon, H. W. W. & Tielens, A. G. G. M., 2004, *ApJ*, 613, 986
- Ptak A., Colbert E., van der Marel R. P.; Roye E., Heckman T. & Towne B., 2006, *ApJS*, 166, 154
- Rigopoulou D. et al., 1996, *A&A*, 315, L125
- Sanders D.B., Egami E., Lípari S., Mirabel I.F. & Soifer B.T., 1995, *AJ*, 110, 1993
- Siebenmorgen R., Krügel E. & Spoon H. W. W., 2004, *A&A*, 414, 123
- Sturm, E., Lutz, D., Tran, D., Feuchtgruber, H., Genzel, R., Kunze, D., Moorwood, A. F. M. & Thornley, M. D., 2000, *A&A*, 358, 481
- Taylor-Mager V. A., Conselice C. J., Windhorst R. A. & Jansen R. A., 2007, *ApJ*, 659, 162
- Verma, A., Lutz, D., Sturm, E., Sternberg, A., Genzel, R. & Vacca, W., 2003, *A&A*, 403, 829
- Zepf S. E., Ashman K. M., English J., Freeman K. C. & Sharples R. M., 1999, *AJ*, 118, 752